

Photoluminescence of metallic single-walled carbon nanotubes: Role of interband and intraband transitions

Takeshi Koyama ^{1,*}, Nobuki Umewaki,¹ Kensuke Saito,¹ Tomoki Tatsuno,¹ Akira Fujisaki,¹
Yasumitsu Miyata ², Hiromichi Kataura ³, and Hideo Kishida ¹

¹*Department of Applied Physics, Nagoya University, Chikusa, Nagoya 464-8603, Japan*

²*Department of Physics, Tokyo Metropolitan University, 1-1 Minami-osawa, Hachioji, Tokyo 192-0397, Japan*

³*Nanomaterials Research Institute,*

National Institute of Advanced Industrial Science and Technology (AIST), Tsukuba, Ibaraki 305-8565, Japan



(Received 20 August 2021; revised 23 June 2022; accepted 5 July 2022; published 25 July 2022)

The photoluminescence (PL) properties of metallic single-walled carbon nanotubes were investigated. Steady-state measurements showed interband excitonic PL in the first hyperbolic dispersion region. The decay kinetics of this interband excitonic PL was observed by femtosecond time-resolved measurements, which also showed the occurrence of intraband PL in the linear dispersion region. The decay time constant of interband excitonic PL is approximately 40 fs, while that of intraband PL is slower at the lower photon energy. This study demonstrates the role of interband and intraband transitions in the PL of a one-dimensional metal.

DOI: [10.1103/PhysRevB.106.045421](https://doi.org/10.1103/PhysRevB.106.045421)

I. INTRODUCTION

Metals have gapless electronic structures where the Coulomb interaction is strongly screened by free carriers. This screening prevents the formation of a bound electron-hole pair, i.e., an exciton, which is a quasiparticle where an electron and a hole are bound by the Coulomb interaction that characterizes the optical properties of semiconductors and insulators. Although transient excitons at metal surfaces have been observed using ultrafast multiphoton photoemission spectroscopy [1], photoluminescence (PL) of metals in most cases originates not from excitons (bound electron-hole pairs) but from free electron-hole pairs (unbound electron-hole pairs), which recombine in interband [2–8] and intraband transitions [6,7,9–11]. However, low dimensionality can suppress the screening effect and thus a relatively stable exciton state is expected to be realized in one-dimensional (1D) metals.

Metallic single-walled carbon nanotubes (SWNTs) are quasi-1D metals [12–15] that exhibit low-dimensional transport properties such as those of Coulomb blockades [16,17] and Tomonaga-Luttinger liquids [18]. The schematic of a band diagram near the Fermi energy of the metallic SWNT is shown in Fig. 1. The red lines indicate linear dispersion bands, with the Fermi energy in the nondoped state situated at the contact point of the upper and lower bands. The blue lines are hyperbolic dispersion curves, which have different quantum numbers from the linear dispersions along the circumferential direction of the nanotube. The exciton associated with the interband transition between the hyperbolic dispersion bands has been theoretically predicted, and its binding energy was calculated to be approximately several tens of meV [19,20]. Exciton formation in metallic SWNTs has also been experimentally investigated by optical absorption [21],

optical reflection [22], Raman scattering [23,24], Rayleigh scattering [25], and PL measurements [26]. The PL measurements of the interband transition between the first hyperbolic dispersion bands established the excitonic nature of this PL and demonstrated an exciton lifetime of 40 ± 10 fs, which has been supported by a recent theoretical study [27].

A linear dispersion, though two dimensional, is formed in graphene, and the interband PL of free electron-hole pairs in the linear dispersion bands has previously been observed [28–36]. However, in the metallic SWNT, the interband transition between the linear dispersion bands is optically forbidden [37–40]. Instead, infrared absorption due to excitation of plasmons with conductive electrons in the linear dispersion bands have been observed [41–45]. It is expected that metallic SWNTs will emit intraband PL in the linear dispersion region with enhancement by plasmon resonance. A recent theoretical study [46] indicated that thermal radiation from metallic SWNTs is a probe of non-Fermi liquid behavior in 1D electron systems and that the radiation in the spectral region below the energy corresponding to the electron temperature is a test for expressions within and beyond the Tomonaga-Luttinger liquid framework. However, it is difficult to observe this radiation as its spectrum is situated in the infrared region, where detector sensitivity is much lower than that in the visible region. Measurements of PL (both hot luminescence and thermal radiation of electron system) in the linear dispersion region of metallic SWNTs have not been performed to date, while electrically driven thermal radiation in the linear dispersion region has been observed up to 1500 nm [47]. In this study, we investigated the PL of metallic SWNTs in both the first hyperbolic dispersion and linear dispersion regions.

II. METHODS

The metallic SWNTs were extracted from SWNT raw materials with the average nanotube diameters of 1.2 and

*Corresponding author: koyama@nuap.nagoya-u.ac.jp

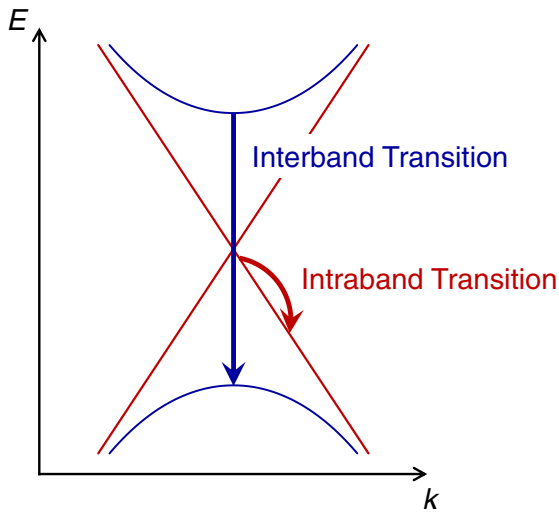


FIG. 1. Schematic of band diagram of a metallic SWNT. The blue curves and red lines indicate hyperbolic and linear dispersion relations, respectively. The blue and red arrows indicate interband and intraband transitions, respectively.

1.4 nm by density gradient ultracentrifugation [48]. The ratios of metallic SWNTs to total SWNTs were determined by comparing the spectral weights of the exciton bands of metallic SWNTs and semiconducting SWNTs in the absorption spectra [48], and the ratios were 0.90, and 0.96 in the aqueous dispersions of the extracted SWNTs for the thick and thin metallic SWNTs, respectively. The dispersions were filtered, and films were formed, where the SWNTs were bundled. The focus of this study was a film of thick metallic SWNTs on filter paper (sample 1). For comparison, thin metallic SWNTs in film form were transferred onto a quartz glass substrate (sample 2). The counterpart semiconducting SWNTs were obtained during the density gradient ultracentrifugation procedure, and a film sample of the semiconducting SWNTs with the average nanotube diameter of 1.4 nm was also prepared on filter paper.

The absorption spectra of the aqueous dispersions were measured using a spectrophotometer (Jasco V-560). The steady-state emission spectra of the film samples were measured using a Raman microspectroscopy instrument (Renishaw inVia) with a He-Ne laser (633 nm, corresponding photon energy 1.96 eV) and a laser diode (488 nm, 2.54 eV). The diameter of the laser beam on the sample was approximately 2 μm . The spectral sensitivity for every experimental setup was calibrated using a standard tungsten lamp. The lamp was placed just at the position of sample to measure the spectrum, and the calibration curve was obtained for a full range of the detection region from 1.56 to 2.53 eV.

The PL decay of the film samples was measured using the frequency up-conversion technique, which is a powerful tool to observe the femtosecond PL decay especially in the infrared region [49,50]. The light source was a mode-locked Ti:sapphire laser [82 MHz, 80 fs, 800 nm (corresponding photon energy 1.55 eV)]. The output of the laser was divided into excitation and gate pulses. The excitation pulse passed through a variable neutral density filter to adjust the excitation

density, and it was focused on the sample. The diameter of the excitation pulse on the sample was approximately 50 μm . The PL from the sample was collected by using a paraboloidal mirror and focused onto a β -barium borated (BBO) crystal by another paraboloidal mirror. Just at the focused position, the gate pulse was directed into the BBO crystal and combined with the PL (sum-frequency generation), converting the frequency to that within the visible or ultraviolet range (frequency up-conversion), which is more easily detected. The sum-frequency light was directed into a monochromator and detected by using a photomultiplier with a photon counting technique. The intensity of the sum-frequency light is proportional to that of the PL. The PL decay curve was obtained by alternately repeating the measurement of the sum-frequency intensity and adjustment of the deference in arrival time at the BBO crystal between the PL and gate pulse, which was changed by moving a delay line in the optical path of the gate pulse.

The instrument response function of the measurement system was determined by measuring the cross-correlation trace between the gate pulse and the excitation pulse scattered from the sample surface. The instrument response function was fitted to a Gaussian function with a full width at half maximum of 140 fs. In the fitting analysis of the PL decay curves, a convolution method with the instrument response function was used to determine the decay time constants with a precision of ± 10 fs. The spectral sensitivity of the system was calibrated by using an infrared standard light source. The sample was replaced by the light source to measure the sum-frequency light. The calibration curve was obtained for the detection region from 0.6 to 1.8 eV. We conducted PL measurements for the quartz glass substrate and filter paper, and found that no PL was observed from the quartz glass substrate, and the signal from the filter paper passing through the SWNT film was time delayed and sufficiently small to be ignored.

III. RESULTS AND DISCUSSION

Figures 2(a) and 2(b) show the emission spectra of sample 1 (average nanotube diameter, 1.4 nm) with excitation densities of 3.1×10^7 and $9.0 \times 10^6 \text{ W s}^{-1}$ at the photon energies of 1.96 and 2.54 eV, respectively. We also measured the spectra with excitation densities of 2.8×10^5 and $3.2 \times 10^6 \text{ W s}^{-1}$ at 1.96 eV. The intensity was proportional to the excitation density, and the spectral shape exhibited no excitation-density dependence, indicating that the observed spectra are in the linear response regime. The spectra in Figs. 2(a) and 2(b) include sharp structures superimposed on a broad structure. To clarify these components, Lorentz functions were fitted. The overall spectra were reproduced well by the black curves, which were decomposed into multiple sharp Lorentz functions and a broad Lorentz function. The peak positions of the sharp functions differ in the two spectra as they correspond to the excitation photon energy, and these components are assigned to the phonon Raman bands of radial breathing mode, intermediate frequency phonon modes, D , G , and G' [51] as well as the multiphonon Raman bands of them [52]. It should be noted that the peak position of the broad function is common in the two spectra, indicating that this component is not a Raman signal.

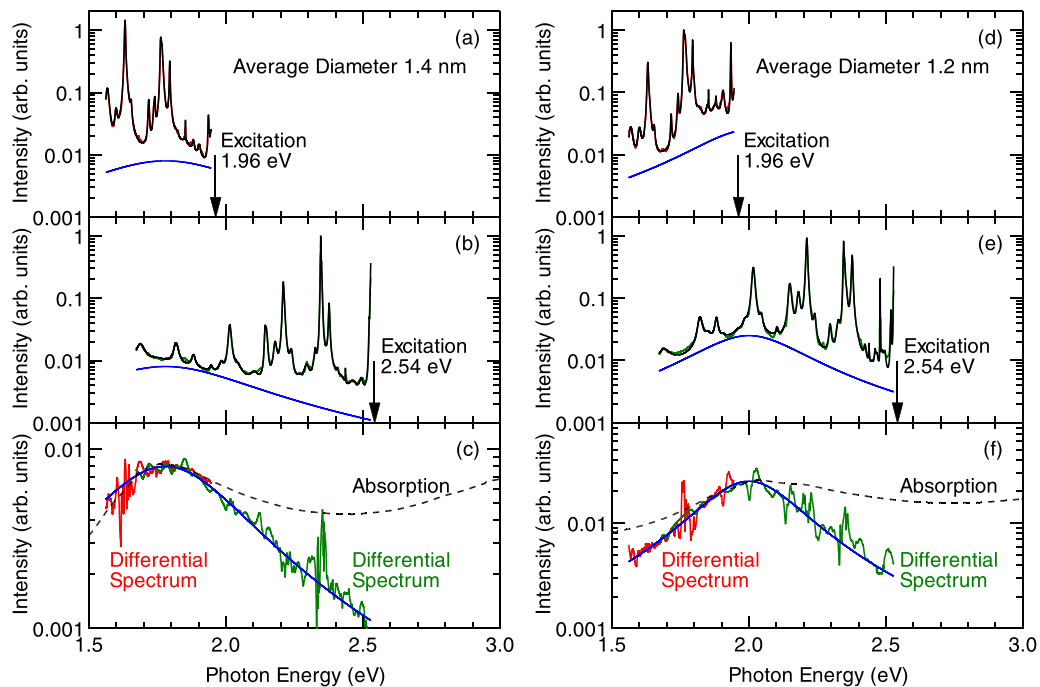


FIG. 2. Emission spectra of sample 1 (average nanotube diameter, 1.4 nm) with an excitation photon energy of (a) 1.96 eV and (b) 2.54 eV, and sample 2 (average nanotube diameter, 1.2 nm) with an excitation energy of (d) 1.96 eV and (e) 2.54 eV. (c),(f) Differential spectra obtained by subtracting sharp structures from the emission spectra with excitation photon energies of 1.96 eV (red) and 2.54 eV (green). The blue curves indicate broad structures. The dashed curves indicate the absorption spectra.

To closely observe the broad component, differential spectra were obtained by subtracting the fitted sharp functions from the observed emission spectra and plotted in Fig. 2(c). The red and green curves correspond to the excitation photon energy of 1.96 and 2.54 eV, respectively. The blue curve indicates the fitted broad function. The peak position and full width at half maximum of the broad component are 1.8 and 0.6 eV, respectively. These are similar to those of an absorption band observed at 1.2–2.3 eV in the absorption spectrum of aqueous dispersion (dashed curve). This absorption band is assigned to an exciton band of the interband transition between the first hyperbolic dispersion bands, i.e., the M_{11} exciton band. It is well known that the interband excitonic PL spectrum of an ensemble of surfactant-wrapped individual semiconducting SWNTs corresponds to the absorption spectrum [53]. Hence, the correspondence of the broad component and the M_{11} exciton band in the absorption spectrum in Fig. 2(c) suggests that the broad component is PL of this exciton band.

Figures 2(d) and 2(e) display the emission spectra of sample 2 (average nanotube diameter, 1.2 nm) with excitation photon energies of 1.96 and 2.54 eV, respectively. As with Figs. 2(a) and 2(b), the spectra were fitted to Lorentz functions, with the overall spectra (black curve) consisting of a common broad Lorentz function with a peak position of 2.0 eV and full width at half maximum of 0.4 eV (blue curve), in addition to multiple sharp Lorentz functions. The differential spectra between the fitted sharp functions and the observed emission spectra with the excitation photon energies of 1.96 eV (red curve) and 2.54 eV (green curve) are plotted in Fig. 2(f) together with the fitted broad function (blue curve). The broad component is consistent with the M_{11} exciton band

(1.4 to 2.5 eV) in the absorption spectrum of sample 2 (dashed curve). This exciton band is situated in the higher energy region than that of sample 1 in Fig. 2(c).

The energy of M_{11} exciton band increases as the nanotube diameter decreases, because the transition energy between the hyperbolic dispersion bands increases with decreasing nanotube diameter [13–15,19,20]. In contrast, the linear dispersion bands are almost independent of the diameter. The nanotube diameter of sample 2 is 1.2 nm and smaller than that of sample 1 (1.4 nm), which explains the higher energy of exciton band of sample 2. The observed broad component in Fig. 2 is consistent with the M_{11} exciton band corresponding to the nanotube diameter. Consequently, the broad component is verified to be the PL of this exciton band.

Figure 3(a) shows the PL decay curves of sample 1 at the emission photon energies of 1.2, 1.3, 1.4, and 1.8 eV in the M_{11} exciton band [see the absorption spectrum of aqueous dispersion in Fig. 3(b)], and also at 0.6, 0.7, 0.8, 0.9, and 1.0 eV. The excitation photon energy is 1.55 eV, which is situated in the M_{11} exciton band, and the excitation density is $3.1 \times 10^{-2} \text{ J m}^{-2}$ per pulse. The intensities in Fig. 3(a) are normalized at the respective maxima of the PL decay curves. All the curves show ultrafast decay, and the intensities become zero within about several hundreds of a femtosecond. The measured results for the film sample of counterpart semiconducting SWNTs are shown by gray curves at 0.7, 1.2, and 1.8 eV. The curves at 0.7 and 1.2 eV show long decay behaviors compared with the corresponding decay curves of the metallic SWNT sample, while the PL at 1.8 eV is not observed. These differences between the two samples indicated that PL from residual semiconducting SWNTs in the metallic SWNT sample was not observed.

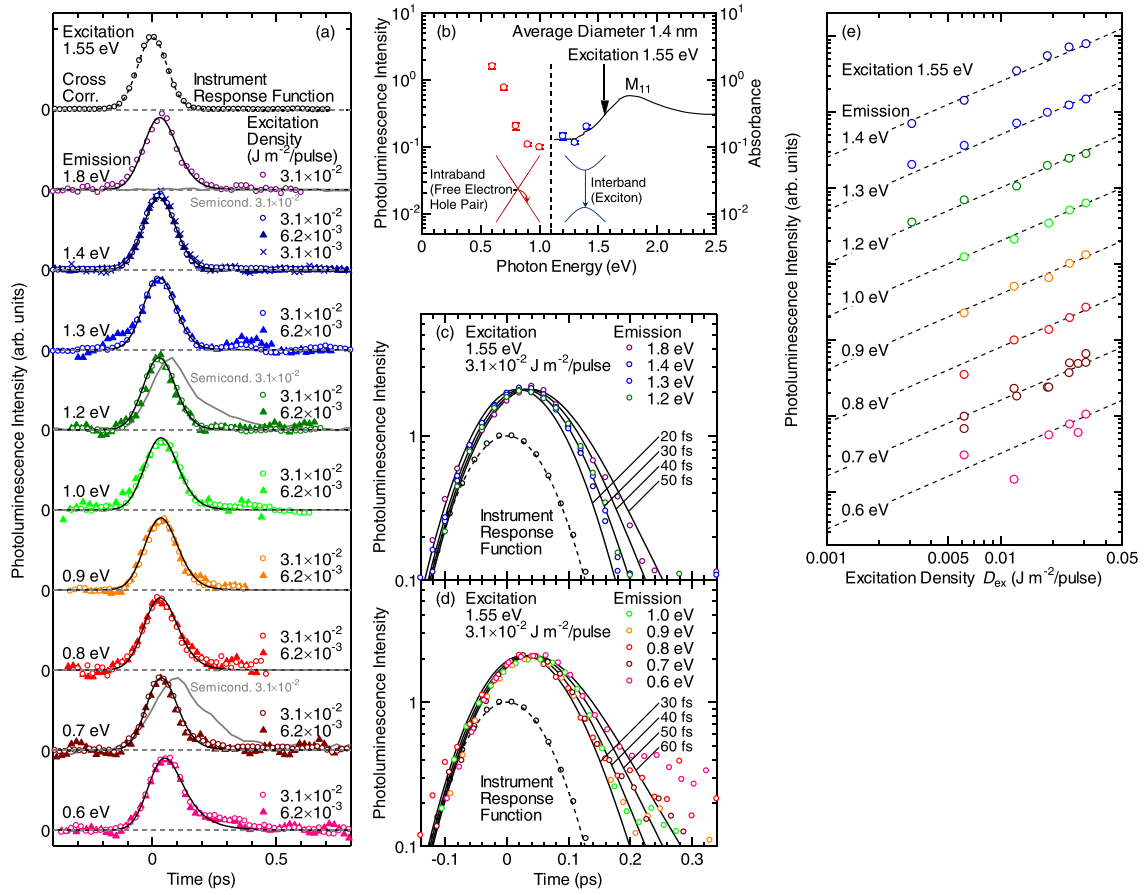


FIG. 3. (a) Cross-correlation trace (instrument response function) and PL decay curves of metallic SWNTs (sample 1) at 0.6, 0.7, 0.8, 0.9, 1.0, 1.2, 1.3, 1.4, and 1.8 eV. Symbols show experimental results; the intensities are normalized at their maxima. The black curves are the fitted results: a Gaussian function for the cross-correlation trace, and single-exponential functions convoluted with the Gaussian function for the PL decay curves. The gray curves show the measured results of PL from the counterpart semiconducting SWNTs at 0.7, 1.2, and 1.8 eV. (b) Photon energy dependence of the maximum intensities of PL decay curves. The excitation density is $3.1 \times 10^{-2} \text{ J m}^{-2}$ per pulse. The solid curve indicates the absorption spectrum of aqueous dispersion. (c),(d) Semilogarithmic plots of instrument response function and PL decay curves of metallic SWNTs (sample 1) at (c) 1.2, 1.3, 1.4, and 1.8 eV and (d) 0.6, 0.7, 0.8, 0.9, and 1.0 eV. Symbols show experimental results. The black dashed curve is the fitted result (Gaussian function) for the instrument response function. The black solid curves are single-exponential functions convoluted with the Gaussian function. The time constants are indicated in the figure. (e) Excitation density dependence of the maximum intensities of PL decay curves at 0.6, 0.7, 0.8, 0.9, 1.0, 1.2, 1.3, and 1.4 eV. The dashed lines indicate linear dependence on the excitation density.

The maximum intensities of the PL decay curves of sample 1 are plotted with respect to the emission photon energy in Fig. 3(b). As the PL at 1.8 eV is an anti-Stokes emission of intensity $\sim 10^{-4} \text{ counts eV}^{-1} \text{ s}^{-1}$, it is out of the frame. Figure 3(b) also shows the absorption spectrum in the range of the M_{11} exciton band above 1.1 eV, with the PL in this range mainly attributed to this exciton band (the details are discussed later). However, the intensity of PL below 1.1 eV increases with decreasing photon energy. This spectral behavior indicates the PL below 1.1 eV cannot be assigned to the M_{11} exciton band. Instead, transitions in the linear dispersion region are involved in such low energy PL (Fig. 1). Since the interband transition between the linear dispersion bands are optically forbidden in the metallic SWNT [37–40], we attribute the PL below 1.1 eV to the intraband PL in the linear dispersion region.

Here, we consider other possibilities of the PL below 1.1 eV. When the light polarization is perpendicular to the

tube axis, the transition between the hyperbolic dispersion band and the linear dispersion band is allowed. If the perpendicularly polarized photoexcitation creates an electron in the hyperbolic conduction band and a hole in the linear valence band, the electron can experience radiative relaxation to the linear conduction band (intersubband transition). This radiative relaxation emits a low energy photon. However, the oscillator strength for the perpendicular polarization is much lower than that for the parallel polarization [40]. Hence, PL with the perpendicularly polarized photoexcitation and emission is ignorable. Another possibility is that the 1.55-eV excitation with parallel polarization generates an exciton, which dissociates into an electron and a hole at the edges of the hyperbolic bands, and the electron (hole) relaxes to the vicinity of the contact point of the linear bands by photon emission with perpendicular polarization. However, infinitely small density of states at the vicinity of the contact point as well as the low oscillator strength for perpendicular polar-

ization of photon emission make the PL due to this radiative relaxation ignorable. Consequently, the possibility of perpendicularly polarized PL is ruled out. In the following, the details of PL of the M_{11} exciton band, i.e., interband excitonic PL in the first hyperbolic dispersion region, and intraband PL in the linear dispersion region are analyzed.

First, we examined the interband excitonic PL in the first hyperbolic dispersion region. Figure 3(c) shows the semilogarithmic plot of the decay curves at 1.2, 1.3, 1.4, and 1.8 eV with the instrument response function. Single-exponential functions with a time constant of 20, 30, 40, and 50 fs (black solid curves) are also plotted after convolution with the instrument response function. The decay curves at 1.2, 1.3, and 1.4 eV are reproduced by the function with a time constant of 30 fs, and that at 1.8 eV is reproduced by the function with a time constant of 40 fs [see also Fig. 3(a) for the linear plot]. These values are consistent with experimentally and theoretically reported lifetimes of excitons in metallic SWNTs [26,27]. As shown in Ref. [26], the recovery of excitonic absorption is longer than the decay of excitonic PL, indicating that unbound electrons and holes survive after the exciton decay with a time constant of 40 fs. Since the excitation photon energy of 1.55 eV is resonant with the M_{11} exciton band, the excitation pulse forms the excitons. The unbound electrons and holes are generated by the exciton dissociation due to exciton-carrier scattering in the time constant of 40 fs, and they survive over this time. It is noted that, as the oscillator strength of excitons is much higher than that of free electron-hole pairs, the excitonic PL is stronger than that of the free electron-hole pairs. Thus, the observed PL decay in this spectral region is mainly attributed to exciton dissociation.

Other possible mechanisms, such as exciton-exciton annihilation (Auger recombination of excitons) [54–57], cannot explain the ultrafast exciton decay. When the excitation density is sufficiently high to generate two excitons closely, the excitons can interact with each other and potentially undergo Auger recombination. In this case, PL decay rapidly becomes fast with increasing excitation density [54,55], whereas no excitation density dependence of the decay behavior is observed in the weak excitation regime [58,59]. Figure 3(a) shows the same decay curves at 1.2, 1.3, and 1.4 eV with excitation densities of 3.1×10^{-2} , 6.2×10^{-3} , and $3.1 \times 10^{-3} \text{ J m}^{-2}$ per pulse, suggesting a weak excitation regime. If the lowest excitation density of $3.1 \times 10^{-3} \text{ J m}^{-2}$ per pulse is still in the region of exciton-exciton annihilation, and it occurs within the time resolution of the experiments, this alternate decay behavior is not observed. In this case, the maximum intensity in the PL decay curve shows sublinear dependence on the excitation density because of the faster decay of excitons [54,55]. In contrast, Fig. 3(e) illustrates the proportionality of the maximum PL intensity to the excitation density. Therefore, under these experimental conditions, exciton-exciton annihilation could not have occurred.

Another possible mechanism is the energy transfer between the SWNTs in a bundle. A previous study demonstrated that the rate of energy transfer in the exciton band from semiconducting SWNTs to neighboring semiconducting SWNTs in a bundle is $1.8\text{--}1.9 \times 10^{12} \text{ s}^{-1}$ [50,60]. As an SWNT is surrounded by six other SWNTs in a bundle, the total rate of transfer from the semiconducting SWNT to the surrounding

semiconducting SWNTs is approximately $1.1 \times 10^{13} \text{ s}^{-1}$, with a corresponding time constant of 90 fs. As the transfer rate is proportional to the spectral overlap between the energy donor and acceptor, and the spectral overlap in the M_{11} exciton band between the metallic SWNTs is similar to or less than that between the semiconducting SWNTs, the time constant of the energy transfer between metallic SWNTs will be 90 fs or more. As this is larger than the observed time constant in Figs. 3(a) and 3(c), this energy transfer cannot explain the observed exciton decay.

Next, the intraband PL in the linear dispersion region is analyzed. Figure 3(a) shows that the decay curves at 0.6, 0.7, 0.8, 0.9, and 1.0 eV with excitation densities of 3.1×10^{-2} and $6.2 \times 10^{-3} \text{ J m}^{-2}$ per pulse are of a similar shape, which is a feature of weak excitation. Figure 3(d) shows the semilogarithmic plot of the decay curves at 0.6, 0.7, 0.8, 0.9, and 1.0 eV with the instrument response function. Single-exponential functions with a time constant of 30, 40, 50, and 60 fs (black solid curves) are also plotted after convolution with the instrument response function. The functions with a time constant of 40 and 60 fs reproduce the decay curves at 0.7–1.0 and 0.6 eV around the time origin, respectively [see also Fig. 3(a)]. Although these curves reflect the experimental results around the time origin, the mismatch between the fitted curves and experimental results especially at 0.6 eV is observed after 0.2 ps, at which point the PL decay can no longer be described by a single-exponential function.

The intraband PL intensity of free electron-hole pairs is proportional to the distribution functions of electrons and holes, which are governed by the carrier temperature after thermalization of the photoexcited carrier system [7,9,10,11]. Cooling of the carrier system occurs due to carrier-phonon scattering leading to the heating of phonon system. After the carrier and phonon temperatures become equal, the decrease in carrier temperature is limited by that of the phonon temperature, that is, the hot phonon bottleneck. Thus, the PL decay slows, and the decay curve cannot be reproduced by a single-exponential function. As the values of the electron and hole distribution functions at high energy approach zero faster than those at low energy, the PL at higher photon energy decays faster. This behavior is observed in the experiments, indicating that the origin of PL in this spectral range is the radiative recombination of free electron-hole pairs. It is noted that, in our experiments, the excitons were formed by the excitation pulse, and then the unbound electrons and holes were generated mainly by the exciton dissociation. Hence, the decay of PL of the free electron-hole pairs was limited by the exciton dissociation, even if electrons and holes underwent the intraband relaxation with the faster time constant. Indeed, the PL at 0.7–1.0 eV around the time origin decayed with a time constant of 40 fs, which is the exciton dissociation time.

The intraband transition is a high-order perturbation process and much weaker than the direct interband transition, which is a first-order perturbation process. However, the PL spectrum in Fig. 3(b) shows strong intraband PL below 0.7 eV compared with the interband excitonic PL. This strong PL can be explained by the enhancement by plasmon resonance. Indeed, the early studies [42,45] showed that a broadband infrared absorption due to plasmon resonance with a peak at 0.06 eV and a high energy tail to 0.8 eV was observed in a

film of metallic SWNTs with the same nanotube diameters and the same purification procedure as our study. The peak of this infrared absorption is 0.7 times as high as the M_{11} exciton peak, and the absorption at 0.6 eV is comparable to those around 1.3 eV. This plasmon resonance effect also causes the enhancement of PL intensity. In addition, the long decay of carrier populations in the low energy region compared with the ultrafast exciton decay causes the large maximum PL intensity in the low energy region.

The lack of excitation density dependence of PL decay in Fig. 3(a) and the linear dependence of PL intensity on the excitation density in Fig. 3(e) indicate that PL in the weak excitation regime is observed in this study. Weak excitation can also be confirmed in terms of the number of absorbed photons per nanotube. The absorption cross section per carbon atom of the M_{11} exciton band in metallic SWNTs is estimated to be $\sim 3 \times 10^{-22} \text{ m}^2$ at 1.55 eV [61]. The length of SWNTs with vigorous sonication used in this study is typically $0.25 \mu\text{m}$ [62]. For a metallic SWNT with a chirality of (18,0), a diameter of 1.4 nm, and a length of $0.25 \mu\text{m}$, the number of carbon atoms in the nanotube is 4.2×10^4 , and the absorption cross section per nanotube is estimated to be $\sim 1 \times 10^{-17} \text{ m}^2$. For the maximum excitation density of $3.1 \times 10^{-2} \text{ J m}^{-2}$ per pulse (1.3×10^{17} photons m^{-2} per pulse), the average number of excitons per nanotube generated is ~ 1 . Consequently, our experimental conditions were in the weak excitation regime.

Here, we estimate the onset excitation density of exciton-exciton annihilation. If the exciton diffusion constant is $5 \text{ cm}^2 \text{ s}^{-1}$ [63], $10.7 \text{ cm}^2 \text{ s}^{-1}$ [64], or $44 \text{ cm}^2 \text{ s}^{-1}$ [65], the same as in a semiconducting SWNT at room temperature, an exciton moves 4.5, 6.5, or 13 nm in the exciton lifetime of 40 fs, respectively. The exciton radius in metallic SWNT is estimated to be $\sim 3 \text{ nm}$ [21]. Hence, when two excitons are excited in a nanotube with a separation of less than $\sim 30 \text{ nm}$, they can interact with each other. This exciton density is expected for the excitation density of $\sim 0.4 \text{ J m}^{-2}$ per pulse ($\sim 2 \times 10^{18}$ photons m^{-2} per pulse), which is the onset of exciton-exciton annihilation in this experimental condition.

Finally, we discuss the impact of low-energy PL in metallic SWNTs. A recent theoretical study indicated that thermal radiation from metallic SWNTs is a probe of non-Fermi liquid behavior in 1D electron systems [46]. In this theoretical study, thermal radiation spectra expressed within and beyond the Tomonaga-Luttinger liquid framework in the case of long quantum coherence demonstrated distinct differences from the black-body radiation in the spectral region below the energy corresponding to the electron temperature. More observations of the emissions in this spectral region are required for further examination. Additionally, ultrashort-pulse photoexcitation can increase the temperature of electron systems until the rise of the electron-phonon coupling (in graphene, an electron temperature exceeding 3000 K achieved by 30-fs pulse excitation with an absorbed fluence of 0.33 J m^{-2} was reported [28]), which will expand the spectral region where the 1D non-Fermi liquid behavior is expected. Hence, PL measurement with such ultrashort strong pulses is a potential method for studying 1D electron liquids and is expected to be performed in the future.

IV. CONCLUSION

In this study, we fabricated film samples of metallic SWNTs and investigated their PL in the M_{11} exciton band and the linear dispersion region. The PL in the M_{11} exciton band decayed with a time constant of 30–40 fs, which is consistent with previous studies. The PL decay in the linear dispersion region is slower at the lower photon energy, which is explained by the cooling of the electron temperature. This study demonstrates the PL of interband and intraband transitions in a 1D metal.

ACKNOWLEDGMENTS

This work was supported by Shorai Foundation for Science and Technology and The Murata Science Foundation.

-
- [1] X. Cui, C. Wang, A. Argondizzo, S. Garrett-Roe, B. Gumhalter, and H. Petek, Transient excitons at metal surfaces, *Nat. Phys.* **10**, 505 (2014).
 - [2] A. Mooradian, Photoluminescence of Metals, *Phys. Rev. Lett.* **22**, 185 (1969).
 - [3] M. Kusunoki, Theory of photoluminescence in metals, *Prog. Theor. Phys.* **47**, 728 (1972).
 - [4] G. T. Boyd, Z. H. Yu, and Y. R. Shen, Photoinduced luminescence from the noble metals and its enhancement on roughened surfaces, *Phys. Rev. B* **33**, 7923 (1986).
 - [5] P. Apell, R. Monreal, and S. Lundqvist, Photoluminescence of noble metals, *Phys. Scr.* **38**, 174 (1988).
 - [6] M. R. Beversluis, A. Bouhelier, and L. Novotny, Continuum generation from single gold nanostructures through near-field mediated intraband transitions, *Phys. Rev. B* **68**, 115433 (2003).
 - [7] T. Haug, P. Klemm, S. Bange, and J. M. Lupton, Hot-Electron Intraband Luminescence from Single Hot Spots in Noble-Metal Nanoparticle Films, *Phys. Rev. Lett.* **115**, 067403 (2015).
 - [8] Y. Sivan and Y. Dubi, Theory of “Hot” photoluminescence from Drude metals, *ACS Nano* **15**, 8724 (2021).
 - [9] T. Suemoto, K. Yamanaka, and N. Sugimoto, Observation of femtosecond infrared luminescence in gold, *Phys. Rev. B* **100**, 125405 (2019).
 - [10] T. Suemoto, K. Yamanaka, N. Sugimoto, T. Otsu, S. Tani, Y. Kobayashi, and T. Koyama, Effect of emissivity on ultrafast luminescence spectra in silver, *J. Appl. Phys.* **128**, 203103 (2020).
 - [11] T. Suemoto, K. Yamanaka, N. Sugimoto, Y. Kobayashi, T. Otsu, S. Tani, and T. Koyama, Relaxation dynamics of hot electrons in transition metals, Au, Ag, Cu, Pt, Pd, and Ni studied by ultrafast luminescence spectroscopy, *J. Appl. Phys.* **130**, 025101 (2021).
 - [12] J. W. Mintmire, B. I. Dunlap, and C. T. White, Are Fullerene Tubules Metallic? *Phys. Rev. Lett.* **68**, 631 (1992).
 - [13] N. Hamada, S. I. Sawada, and A. Oshiyama, New One-Dimensional Conductors: Graphitic Microtubules, *Phys. Rev. Lett.* **68**, 1579 (1992).

- [14] K. Tanaka, K. Okahara, M. Okada, and T. Yamabe, Electronic properties of bucky-tube model, *Chem. Phys. Lett.* **191**, 469 (1992).
- [15] R. Saito, M. Fujita, G. Dresselhaus, and M. S. Dresselhaus, Electronic structure of chiral graphene tubules, *Appl. Phys. Lett.* **60**, 2204 (1992).
- [16] S. J. Tans, M. D. Devoret, H. Dai, A. Thess, R. E. Smalley, L. J. Geerligs, and C. Dekker, Individual single-wall carbon nanotubes as quantum wires, *Nature (London)* **386**, 474 (1997).
- [17] M. Bockrath, D. H. Cobden, P. L. McEuen, N. G. Chopra, A. Zettl, A. Thess, and R. E. Smalley, Single-electron transport in ropes of carbon nanotubes, *Science* **275**, 1922 (1997).
- [18] H. Ishii, H. Kataura, H. Shiozawa, H. Yoshioka, H. Otsubo, Y. Takayama, T. Miyahara, S. Suzuki, Y. Achiba, M. Nakatake, T. Narimura, M. Higashiguchi, K. Shimada, H. Namatame, and M. Taniguchi, Direct observation of Tomonaga-Luttinger-liquid state in carbon nanotubes at low temperatures, *Nature (London)* **426**, 540 (2003).
- [19] T. Ando, Excitons in carbon nanotubes, *J. Phys. Soc. Jpn.* **66**, 1066 (1997).
- [20] C. D. Spataru, S. Ismail-Beigi, L. X. Benedict, and S. G. Louie, Excitonic Effects and Optical Spectra of Single-Walled Carbon Nanotubes, *Phys. Rev. Lett.* **92**, 077402 (2004).
- [21] F. Wang, D. J. Cho, B. Kessler, J. Deslippe, P. J. Schuck, S. G. Louie, A. Zettl, T. F. Heinz, and Y. R. Shen, Observation of Excitons in One-Dimensional Metallic Single-Walled Carbon Nanotubes, *Phys. Rev. Lett.* **99**, 227401 (2007).
- [22] H. Zeng, H. Zhao, F.-C. Zhang, and X. Cui, Observation of Exciton-Phonon Sideband in Individual Metallic Single-Walled Carbon Nanotubes, *Phys. Rev. Lett.* **102**, 136406 (2009).
- [23] S. K. Doorn, P. T. Araujo, K. Hata, and A. Jorio, Excitons and exciton-phonon coupling in metallic single-walled carbon nanotubes: Resonance Raman spectroscopy, *Phys. Rev. B* **78**, 165408 (2008).
- [24] P. May, H. Telg, G. Zhong, J. Robertson, C. Thomsen, and J. Maultzsch, Observation of excitonic effects in metallic single-walled carbon nanotubes, *Phys. Rev. B* **82**, 195412 (2010).
- [25] S. Berciaud, C. Voisin, H. Yan, B. Chandra, R. Caldwell, Y. Shan, L. E. Brus, J. Hone, and T. F. Heinz, Excitons and high-order optical transitions in individual carbon nanotubes: A Rayleigh scattering spectroscopy study, *Phys. Rev. B* **81**, 041414(R) (2010).
- [26] T. Koyama, S. Shimizu, T. Saito, Y. Miyata, H. Shinohara, and A. Nakamura, Ultrafast luminescence kinetics of metallic single-walled carbon nanotubes: Possible evidence for excitonic luminescence, *Phys. Rev. B* **85**, 045428 (2012).
- [27] L. Shan, M. Agarwal, and E. G. Mishchenko, Binding energy and lifetime of excitons in metallic nanotubes, *Phys. Rev. B* **99**, 035434 (2019).
- [28] C. H. Lui, K. F. Mak, J. Shan, and T. F. Heinz, Ultrafast Photoluminescence from Graphene, *Phys. Rev. Lett.* **105**, 127404 (2010).
- [29] W.-T. Liu, S. W. Wu, P. J. Schuck, M. Salmeron, Y. R. Shen, and F. Wang, Nonlinear broadband photoluminescence of graphene induced by femtosecond laser irradiation, *Phys. Rev. B* **82**, 081408(R) (2010).
- [30] R. J. Stöhr, R. Kolesov, J. Pflaum, and J. Wrachtrup, Fluorescence of laser-created electron-hole plasma in graphene, *Phys. Rev. B* **82**, 121408(R) (2010).
- [31] C.-F. Chen, C.-H. Park, B. W. Boudouris, J. Horng, B. Geng, C. Girit, A. Zettl, M. F. Crommie, R. A. Segalman, S. G. Louie, and F. Wang, Controlling inelastic light scattering quantum pathways in graphene, *Nature (London)* **471**, 617 (2011).
- [32] T. Koyama, Y. Ito, K. Yoshida, M. Tsuji, H. Ago, H. Kishida, and A. Nakamura, Near-infrared photoluminescence in the femtosecond time region in monolayer graphene on SiO₂, *ACS Nano* **7**, 2335 (2013).
- [33] H. Watanabe, T. Kawasaki, T. Iimori, F. Komori, and T. Suemoto, Layer number dependence of carrier lifetime in graphenes observed using time-resolved mid-infrared luminescence, *Chem. Phys. Lett.* **637**, 58 (2015).
- [34] H. Imaeda, T. Koyama, H. Kishida, K. Kawahara, H. Ago, R. Sakakibara, W. Norimatsu, T. Terasawa, J. Bao, and M. Kusunoki, Acceleration of photocarrier relaxation in graphene achieved by epitaxial growth: Ultrafast photoluminescence decay of monolayer graphene on SiC, *J. Phys. Chem. C* **122**, 19273 (2018).
- [35] D. Huang, T. Jiang, Y. Zhang, Y. Shan, X. Fan, Z. Zhang, Y. Dai, L. Shi, K. Liu, C. Zeng, J. Zi, W.-T. Liu, and S. Wu, Gate switching of ultrafast photoluminescence in graphene, *Nano Lett.* **18**, 7985 (2018).
- [36] K. Saito, T. Koishi, J. Bao, W. Norimatsu, M. Kusunoki, H. Kishida, and T. Koyama, Photoluminescence enhancement exceeding 10-fold from graphene via an additional layer: Photoluminescence from monolayer and bilayer graphene epitaxially grown on SiC, *J. Phys. Chem. C* **125**, 11014 (2021).
- [37] H. Ajiki and T. Ando, Aharonov-Bohm effect in carbon nanotubes, *Phys. B (Amsterdam, Neth.)* **201**, 349 (1994).
- [38] J. Jiang, R. Saito, A. Grüneis, G. Dresselhaus, and M. S. Dresselhaus, Optical absorption matrix elements in single-wall carbon nanotubes, *Carbon* **42**, 3169 (2004).
- [39] T. Ando, Theory of electronic states and transport in carbon nanotubes, *J. Phys. Soc. Jpn.* **74**, 777 (2005).
- [40] S. Uryu and T. Ando, Excitons in metallic carbon nanotubes with Aharonov-Bohm flux, *Phys. Rev. B* **77**, 205407 (2008).
- [41] N. Akima, Y. Iwasa, S. Brown, A. M. Barbour, J. Cao, J. L. Musfeldt, H. Matsui, M. Shiraishi, H. Shimoda, and O. Zhou, Strong anisotropy in the far-infrared absorption spectra of stretch-aligned single-walled carbon nanotubes, *Adv. Mater.* **18**, 1166 (2006).
- [42] M. Ichida, S. Saito, T. Nakano, Y. Feng, Y. Miyata, K. Yanagi, H. Kataura, and H. Ando, Absorption spectra of high purity metallic and semiconducting single-walled carbon nanotube thin films in a wide energy region, *Solid State Commun.* **151**, 1696 (2011).
- [43] T. Morimoto, S.-K. Joung, T. Saito, D. N. Futaba, K. Hata, and T. Okazaki, Length-dependent plasmon resonance in single-walled carbon nanotubes, *ACS Nano* **8**, 9897 (2014).
- [44] Z. Shi, X. Hong, H. A. Bechtel, B. Zeng, M. C. Martin, K. Watanabe, T. Taniguchi, Y.-R. Shen, and F. Wang, Observation of Luttinger-liquid plasmon in metallic single-walled carbon nanotubes, *Nat. Photonics* **9**, 515 (2015).
- [45] M. Ichida, K. Nagao, Y. Ikemoto, T. Okazaki, Y. Miyata, A. Kawakami, H. Kataura, I. Umezu, and H. Ando, E-beam irradiation effects on IR absorption bands in single-walled carbon nanotubes, *Solid State Commun.* **250**, 119 (2017).
- [46] W. DeGottardi, M. J. Gullans, S. Hegde, S. Vishveshwara, and M. Hafezi, Thermal radiation as a probe of one-dimensional electron liquids, *Phys. Rev. B* **99**, 235124 (2019).

- [47] Z. Liu, A. Bushmaker, M. Aykol, and S. B. Cronin, Thermal emission spectra from individual suspended carbon nanotubes, *ACS Nano* **5**, 4634 (2011).
- [48] Y. Miyata, K. Yanagi, Y. Maniwa, and H. Kataura, Optical evaluation of the metal-to-semiconductor ratio of single-wall carbon nanotubes, *J. Phys. Chem. C* **112**, 13187 (2008).
- [49] T. Koyama and T. Suemoto, Dynamics of nuclear wave packets at the F center in alkali halides, *Rep. Prog. Phys.* **74**, 076502 (2011).
- [50] T. Koyama, Y. Miyata, K. Asaka, H. Shinohara, Y. Saito, and A. Nakamura, Ultrafast energy transfer of one-dimensional excitons between carbon nanotubes: A femtosecond time-resolved luminescence study, *Phys. Chem. Chem. Phys.* **14**, 1070 (2012).
- [51] M. S. Dresselhaus, G. Dresselhaus, R. Saito, and A. Jorio, Raman spectroscopy of carbon nanotubes, *Phys. Rep.* **409**, 47 (2005).
- [52] F. Wang, W. Liu, Y. Wu, M. Y. Sfeir, L. Huang, J. Hone, S. O'Brien, L. E. Brus, T. F. Heinz, and Y. R. Shen, Multiphonon Raman Scattering from Individual Single-Walled Carbon Nanotubes, *Phys. Rev. Lett.* **98**, 047402 (2007).
- [53] M. J. O'Connell, S. M. Bachilo, C. B. Huffman, V. C. Moore, M. S. Strano, E. H. Haroz, K. L. Rialon, P. J. Boul, W. H. Noon, C. Kittrell, J. Ma, R. H. Hauge, R. B. Weisman, and R. E. Smalley, Band gap fluorescence from individual single-walled carbon nanotubes, *Science* **297**, 593 (2002).
- [54] Y.-Z. Ma, J. Stenger, J. Zimmermann, S. M. Bachilo, R. E. Smalley, R. B. Weisman, and G. R. Fleming, Ultrafast carrier dynamics in single-walled carbon nanotubes probed by femtosecond spectroscopy, *J. Chem. Phys.* **120**, 3368 (2004).
- [55] F. Wang, G. Dukovic, E. Knoesel, L. E. Brus, and T. F. Heinz, Observation of rapid Auger recombination in optically excited semiconducting carbon nanotubes, *Phys. Rev. B* **70**, 241403(R) (2004).
- [56] T. Koyama, Y. Miyata, H. Kishida, H. Shinohara, and A. Nakamura, Photophysics in single-walled carbon nanotubes with (6,4) chirality at high excitation densities: Bimolecular Auger recombination and phase-space filling of excitons, *J. Phys. Chem. C* **117**, 1974 (2013).
- [57] T. Koyama, S. Yoshimitsu, Y. Miyata, H. Shinohara, H. Kishida, and A. Nakamura, Transient absorption kinetics associated with higher exciton states in semiconducting single-walled carbon nanotubes: Relaxation of excitons and phonons, *J. Phys. Chem. C* **117**, 20289 (2013).
- [58] H. Hirori, K. Matsuda, Y. Miyauchi, S. Maruyama, and Y. Kanemitsu, Exciton Localization of Single-Walled Carbon Nanotubes Revealed by Femtosecond Excitation Correlation Spectroscopy, *Phys. Rev. Lett.* **97**, 257401 (2006).
- [59] A. Högele, C. Galland, M. Winger, and A. Imamoğlu, Photon Antibunching in the Photoluminescence Spectra of a Single Carbon Nanotube, *Phys. Rev. Lett.* **100**, 217401 (2008).
- [60] T. Koyama, K. Asaka, N. Hikosaka, H. Kishida, Y. Saito, and A. Nakamura, Ultrafast exciton energy transfer in bundles of single-walled carbon nanotubes, *J. Phys. Chem. Lett.* **2**, 127 (2011).
- [61] M. F. Islam, D. E. Milkie, C. L. Kane, A. G. Yodh, and J. M. Kikkawa, Direct Measurement of the Polarized Optical Absorption Cross Section of Single-Wall Carbon Nanotubes, *Phys. Rev. Lett.* **93**, 037404 (2004).
- [62] Y. Miyata, K. Shiozawa, Y. Asada, Y. Ohno, R. Kitaura, T. Mizutani, and H. Shinohara, Length-sorted semiconducting carbon nanotubes for high-mobility thin film transistors, *Nano Res.* **4**, 963 (2011).
- [63] J. Xie, T. Inaba, R. Sugiyama, and Y. Homma, Intrinsic diffusion length of excitons in long single-walled carbon nanotubes from photoluminescence spectra, *Phys. Rev. B* **85**, 085434 (2012).
- [64] T. Hertel, S. Himmelein, T. Ackermann, D. Stich, and J. Crochet, Diffusion limited photoluminescence quantum yields in 1-D semiconductor: Single-wall carbon nanotubes, *ACS Nano* **4**, 7161 (2010).
- [65] S. Moritsubo, T. Murai, T. Shimada, Y. Murakami, S. Chiashi, S. Maruyama, and Y. K. Kato, Exciton Diffusion in Air-Suspended Single-Walled Carbon Nanotubes, *Phys. Rev. Lett.* **104**, 247402 (2010).